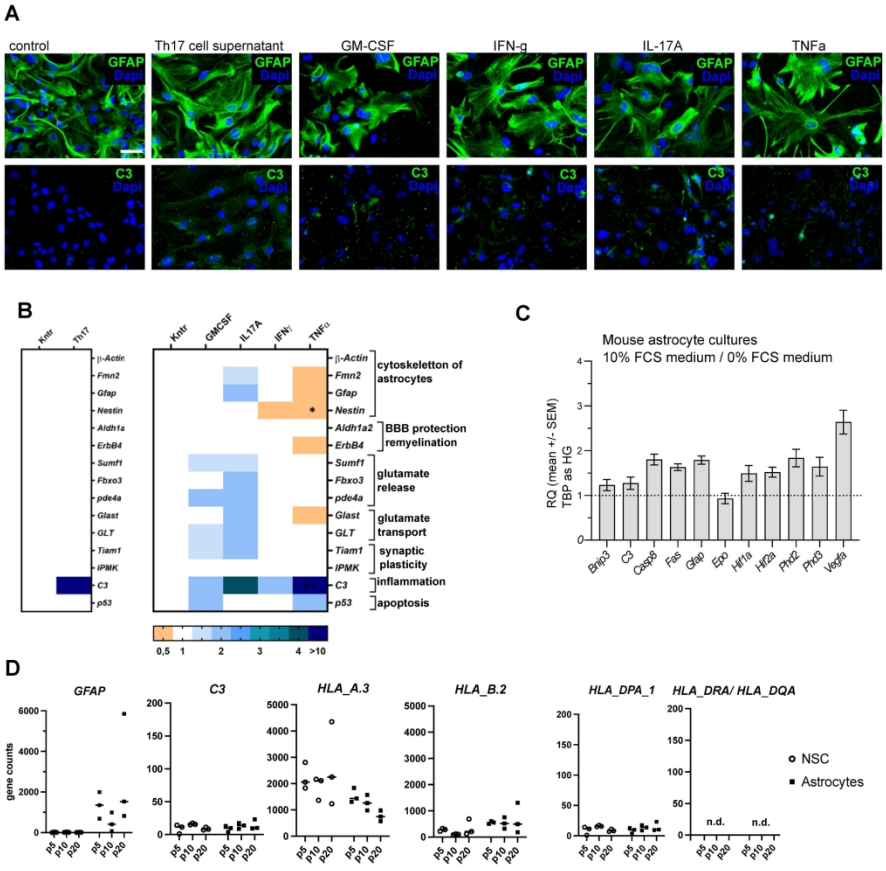

Fig. S1 Astrocytes at baseline of in vitro assays show no clear signs of activation
A C3 IF analysis as marker for A1 astrocytes: mouse astrocytes were stimulated with Th17 cell conditioned media containing 10% FCS or the indicated cytokines (50 ng/ml) for 48h. Cells were fixed and stained for GFAP and complement C3. **B** rt-qPCR of Th17-conditioned medium-treated astrocyte cultures confirmed *C3* upregulation. Astrocyte cultures exposed to different cytokines (50 ng/ml) revealed distinct patterns of activation (all upregulating A1-marker C3; TBP as HG); n = 3, p-values: * < 0.05, ** < 0.01, Kruskal-Wallis test. **C** Mouse astrocytes grown in 10% FCS medium showed increased transcription of observed genes in comparison to mouse astrocytes deprived of FCS (the latter as used for assays in Fig. 1; all in normoxia conditions).
D Human (H9-derived) astrocytes generated in 1% FCS (astrocyte) medium underwent NGS (details of the procedures in Alisch et al., J. Neurosc. Methods 2021). Gene count analysis for selected reactivity-related astrocyte genes (Escartin, Nat. Neurosc. 2021; Perriot, Stem Cell Reports 2018) did not show enhanced expression compared to NSC (except for lineage marker GFAP). In particular *HLA-DR* and *HLA-DQ* were not detectable.

200x272mm (300 x 300 DPI)

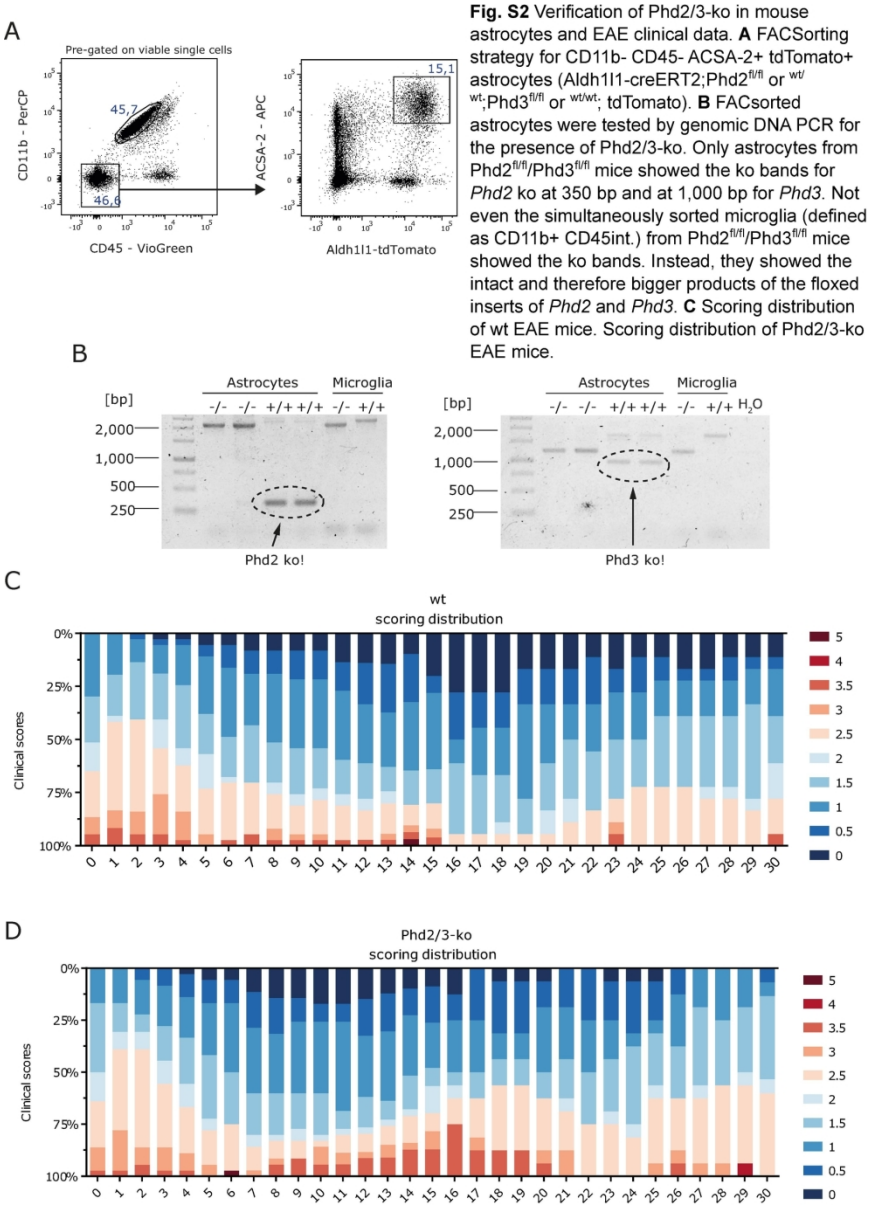

Fig. S2 Verification of Phd2/3-ko in mouse astrocytes and EAE clinical data. **A** FACSorting strategy for CD11b- CD45- ACSA-2+ tdTomato+ astrocytes (Aldh1l1-creERT2;$Phd2^{fl/fl}$ or $^{wt/wt}$;$Phd3^{fl/fl}$ or $^{wt/wt}$; tdTomato). **B** FACsorted astrocytes were tested by genomic DNA PCR for the presence of Phd2/3-ko. Only astrocytes from $Phd2^{fl/fl}$/$Phd3^{fl/fl}$ mice showed the ko bands for *Phd2* ko at 350 bp and at 1,000 bp for *Phd3*. Not even the simultaneously sorted microglia (defined as CD11b+ CD45int.) from $Phd2^{fl/fl}$/$Phd3^{fl/fl}$ mice showed the ko bands. Instead, they showed the intact and therefore bigger products of the floxed inserts of *Phd2* and *Phd3*. **C** Scoring distribution of wt EAE mice. Scoring distribution of Phd2/3-ko EAE mice.

151x210mm (300 x 300 DPI)

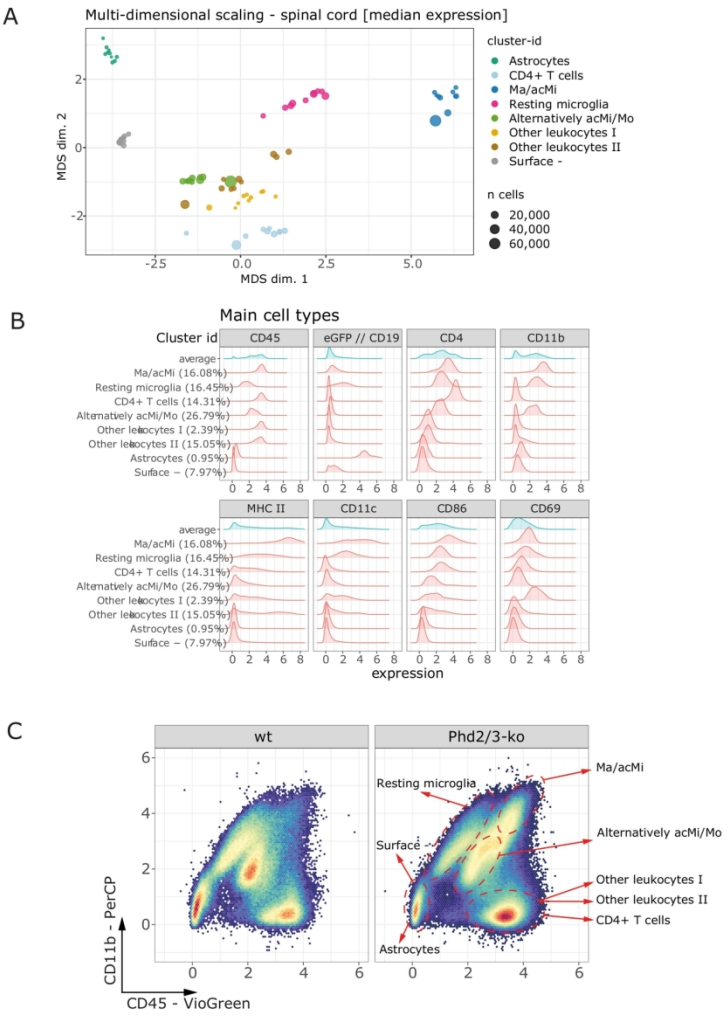

Fig. S3 Expression pattern of defined cell cluster isolated from spinal cords. **A** Multi-dimensional scaling (MDS) plot based on median marker expression shows a clear separation of most cluster. Here, all samples from wt and Phd2/3-ko animals were pooled. **B** Histogram marker expression per defined cluster. **C** Conventional scatter plot for CD11b / CD45 marker expression. Location of cluster assigned cells is visualized by red dashed circles. Concatenated data.

157x222mm (300 x 300 DPI)

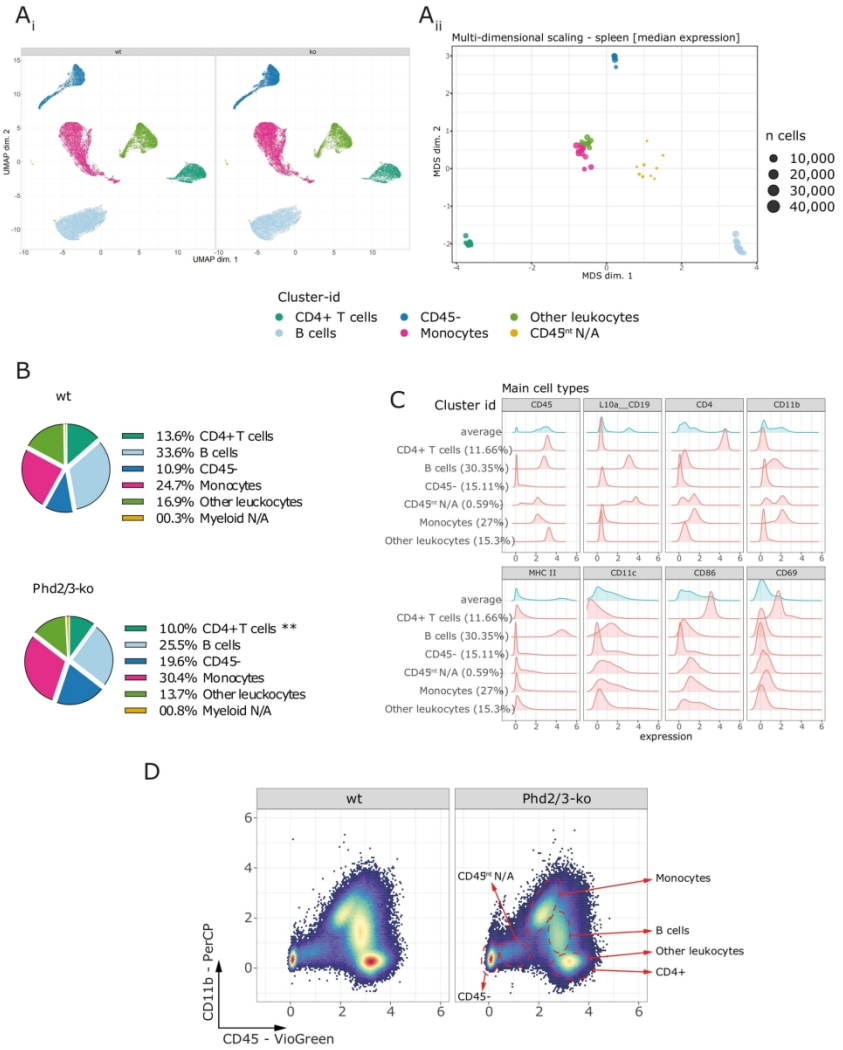

Fig. S4 Expression pattern of defined cell cluster isolated from spinal cords. **A** Multi-dimensional scaling (MDS) plot based on median marker expression shows a clear separation of most cluster. Here, all samples from wt and Phd2/3-ko animals were pooled. **B** Histogram marker expression per defined cluster. **C** Conventional scatter plot for CD11b / CD45 marker expression. Location of cluster assigned cells is visualized by red dashed circles. Concatenated data.

157x222mm (300 x 300 DPI)

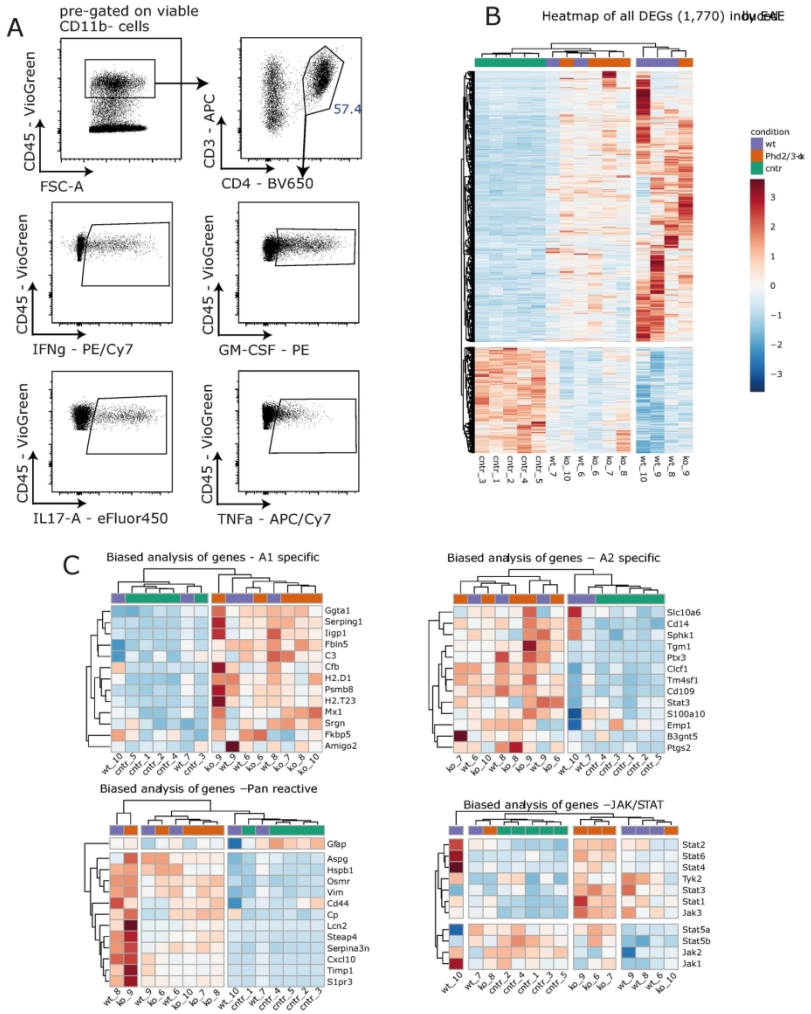

Fig. S5 Cytokine expression in CD4+ T cells and gene expression analysis of astrocytes. **A** Gating strategy for the flow cytometric analysis of the cytokine expression in spinal cord and spleen isolated cells. **B** Expression pattern of EAE induced 1,770 DEGs (p = <0.05) based on the statistical analysis between naïve control group and wt EAE group. **C** Gene expression results from the biased analysis. Most EAE mice had astrocytes of an A1, A2 and an overall pan reactive phenotype. Astrocytes from a group of Phd2/3-ko animals showed also upregulated JAK/STAT pathways. All expression pattern are color coded. Heatmap scale is shown on the right.

140x201mm (300 x 300 DPI)

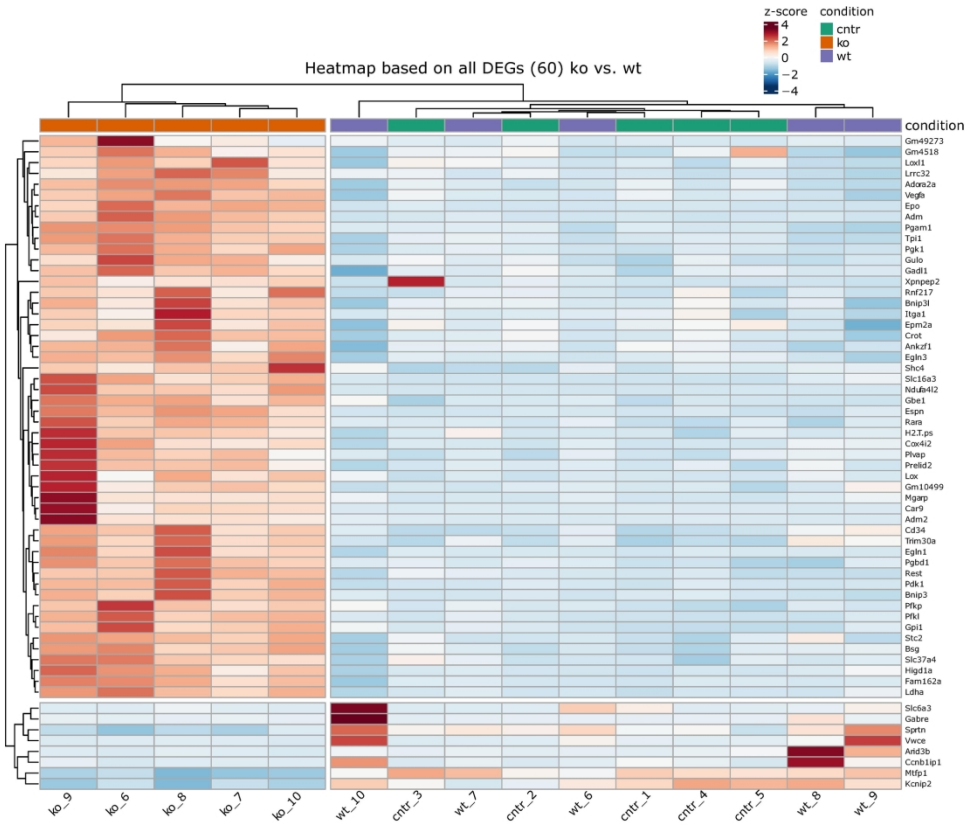

Fig. S6 Top differentially expressed genes between the 3 groups of astrocytes isolated from Phd2/3-ko EAE, Phd2/3-wt EAE and Phd2/3-wt control animals. This heatmap is made up of the 60 DEGs from Phd2/3-ko EAE vs. Phd2/3-wt EAE. The Phd2/3-ko EAE samples separate from Phd2/3-wt control and Phd2/3-wt-EAE samples. Comparing Phd2/3-ko EAE vs. Phd2/3-wt control showed us 1,275 DEGs ($p < 0.05$). Comparing Phd2/3-ko EAE vs. Phd2/3-wt EAE, we found 60 DEGs. Next, comparing DEGs ($p < 0.05$) between Phd2/3-ko EAE vs. Phd2/3-wt control 56 of the 60 DEGs from Phd2/3-ko vs. wt turned up again. This means in turn, that 93.3% of these 60 DEGs between Phd2/3-ko EAE vs. Phd2/3-wt EAE were directly related to the KO of Phd2/3 rather than EAE related.

192x202mm (300 x 300 DPI)

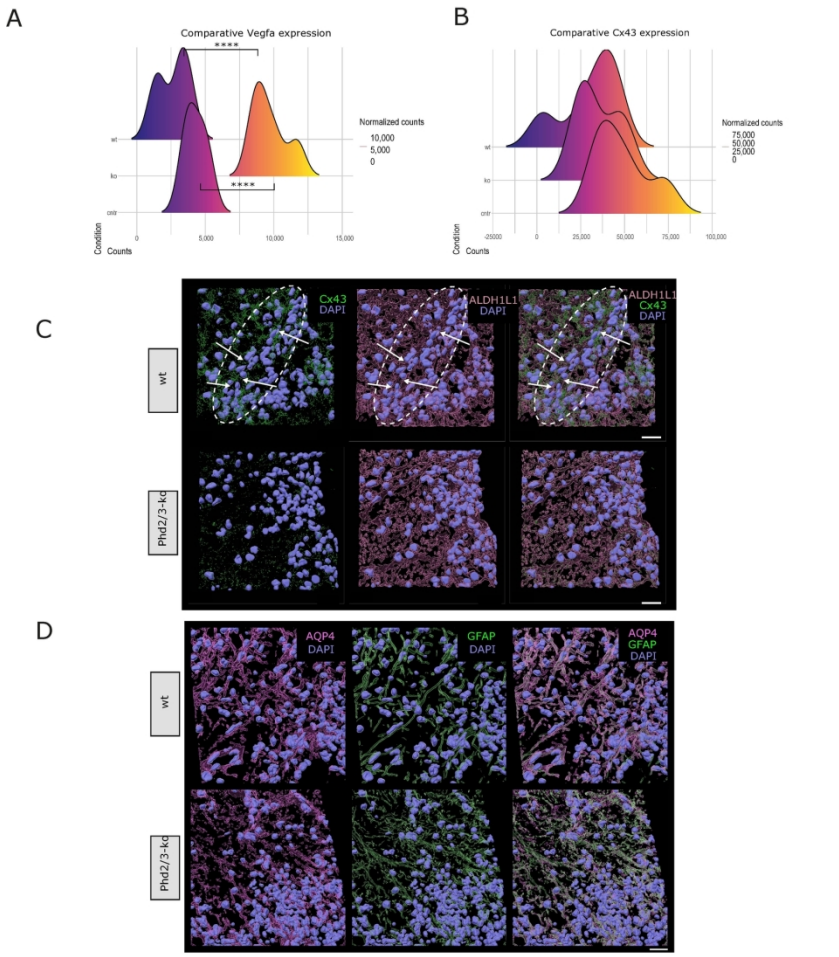

Fig. S7 Gene expression analysis and confocal imaging of important hypoxia and astrocytic syncitium player during EAE. **A** Comparative gene expression of Vegfa (**A**) and Cx43 (**B**). The Phd2/3-ko seems to have only a direct impact on the expression level of Vegfa (strong upregulation), but not on Cx43. Naïve control n= 5, wt n = 5, Phd2/3-ko n= 5. **C** Confocal imaging and 3D reconstruction of ROIs of the same EAE samples shown in Fig. 6 C+D visualized Cx43´s decreased protein expression in acute lesions of Phd2/3-ko animals. The dashed line indicate an area of a vessel cuff with high amounts of peripheral immune cell infiltrates accompanied by a high Cx43 expression in a wt animal. Representative images of each experimental group. White bars 100 µm. **D** Samples from the same EAE animals were used for confocal imaging and 3D reconstruction to visualize periva-scular astrocytes by the staining of AQP4 and GFAP. Representative images of each experimental group. White bars 100 µm.

146x212mm (300 x 300 DPI)

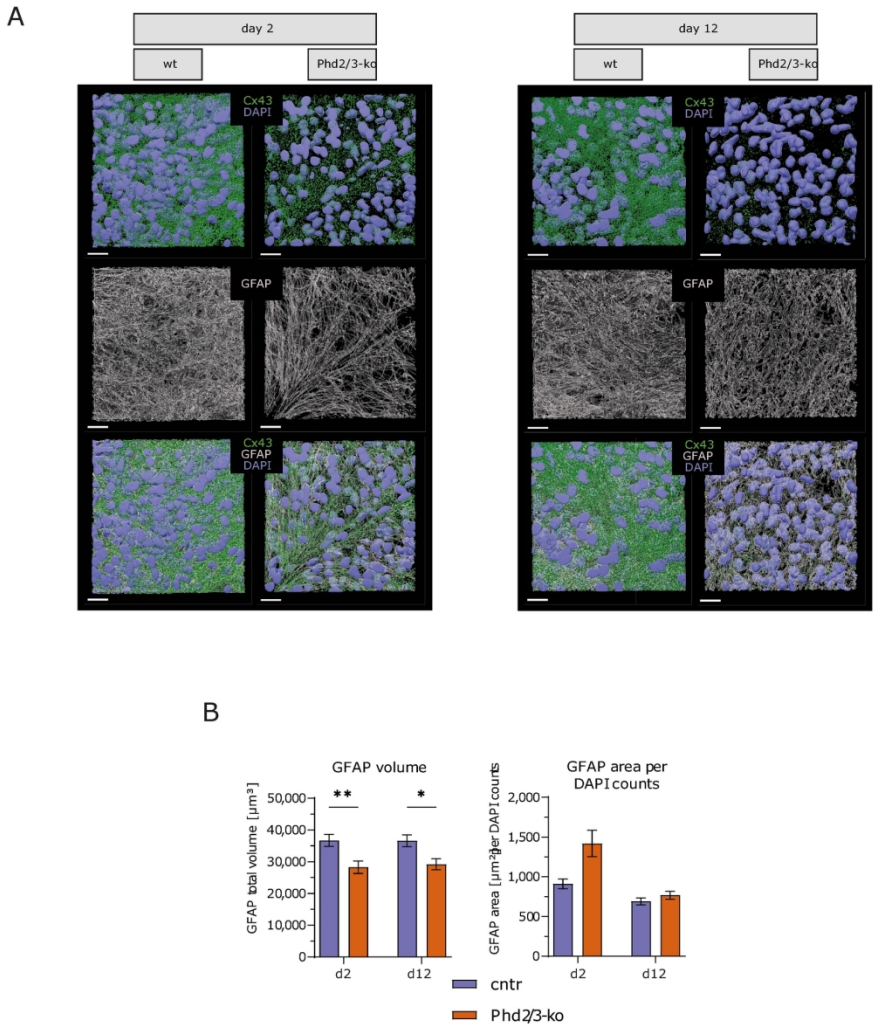

Fig. S8 Protein expression of GFAP in in vitro cultivated brain slices. **A** 3D reconstructed microscopy scans of mouse brain slices 2 days and 12 days after first 4-OH Tamoxifen application. **B** Quantitative analysis of microscopy data showed decreased GFAP volumes in brain slices with an astrocyte directed Phd2/3-ko. n brain slices d2, control = 8, Phd2/3-ko = 7; n brain slices d12, control = 3, Phd2/3-ko = 4. In total 23 ROIs per experimental group and day were microscoped and analyzed. Bar graphs are presen-ted as means with SEM. Statistical analysis was performed by Kruskal-Wallis test corrected by Dunn´s multiple comparison test.

146x198mm (300 x 300 DPI)

Tab1. Mouse phenotypic data

Genotype	Age at immunization (weeks)	p^1	Day of treatment start	p^1	Treated mice	females	males	p^2
wt	20.0 (± 1.4)	0.71	15.0 (± 0.5)	0.71	37	43.2 %	56.8 %	0.35
Phd2/3-ko	19.5 (± 1.2)		15.0 (± 0.4)		36	55.6 %	44.4 %	

Genotype	Incidence	p^2	Mean clinical score at the start of treatment	p^1	Max. clinical score after treatment start (mean)	p^1	Min. clinical score after treatment start (mean)	p^1
wt	69.8 %	0.99	1.8 (± 0.13)	0.52	2.6 (± 0.1)	0.11	0.8 (± 0.1)	0.55
Phd2/3-ko	69.2 %		1.9 (± 0.1)		2.8 (± 0.1)		0.7 (± 0.1)	

147x86mm (300 x 300 DPI)

Tab. 2 qPCR primer - human

Gene	Forward primer	Reverse primer	Amplicon size [bp]
Hif1a	GAACGTCGAAAAGAAAAGTCTCG	CCTTATCAAGATGCGAACTCACA	124
Hif2a	GGACTTACACAGGTGGAGCTA	TCTCACGAATCTCCTCATGGT	79
Phd2	AGGCGATAAGATCACCTGGAT	TTCGTCCGGCCATTGATTTTG	135
Phd3	CTGGGCAAATACTACGTCAAGG	GACCATCACCGTTGGGGTT	106
Epo	AGGCCCTGTTGGTCAACTCT	GCAGTGATTGTTCGGAGTGGA	172
Vegfa	AGGGCAGAATCATCACGAAGT	AGGGTCTCGATTGGATGGCA	75
Bnip3	CAGGGCTCCTGGGTAGAACT	CTACTCCGTCCAGACTCATGC	131
Fas	TCTGGTTCTTACGTCTGTTGC	CTGTGCAGTCCCTAGCTTTCC	197
Casp8	GTTGTGTGGGGTAATGACAATCT	TCAAAGGTCGTGGTCAAAGCC	222
Rest	ACTCAGCGTCGTAGAACCTCA	CGAAAGGGTTTGGTCTTCGAG	135
Adora2a	CATGCTAGGTTGGAACAACTGC	AGATCCGCAAATAGACACCCA	185
Pdk1	GAGAGCCACTATGGAACACCA	GGAGGTCTCAACACGAGGT	187
Cd34	CTACAACACCTAGTACCCTTGGA	GGTGAACACTGTGCTGATTACA	185
Gfap	ATCAACTCACCGCCAACAGCGCC	CTCATACTGCGTGCGGATCTCTT	347
Tbp	CCACTCACAGACTCTCACAAC	CTGCGGTACAATCCCAGAACT	127

Tab. 3 qPCR Primer - mouse

Gene	Forward primer	Reverse primer	Amplicon size [bp]
Hif1a	ACCTTCATCGGAAACTCCAAAG	CTGTTAGGCTGGGAAAAGTTAGG	228
Hif2a	CTGAGGAAGGAGAAATCCCGT	TGTGTCCGAAGGAAGCTGATG	161
Phd2	GATAAACGGCCGAACGAAA	CATGTCACGCATCTTCCATC	105
Phd3	AGGCAATGGTGGCTTGCTATC	GCGTCCCAATTCTTATTCAGGT	118
Epo	ACTCTCCTTGCTACTGATTCCT	ATCGTGACATTTTCTGCCTCC	123
Vegfa	GCACATAGAGAGAATGAGCTTCC	CTCCGCTCTGAACAAGGCT	105
Bnip3	TCCTGGGTAGAACTGCACTTC	GCTGGGCATCCAACAGTATTT	103
Fas	GCGGGTTCGTGAAACTGATAA	GCAAAATGGGCCTCCTTGATA	61
Casp8	TGCTTGGACTACATCCCACAC	TGCAGTCTAGGAAGTTGACCA	169
Rest	AACCCCAGCCCGTATTTGAAG	TGGCCTTAGAACTCCTGCATT	111
Adora2a	GCCATCCCATTCGCCATCA	GCAATAGCCAAGAGGCTGAAGA	122
Pdk1	GCACTCCTTATTGTTCGGTGG	CGTCGCAGTTTGGATTTATGCT	77
Cd34	AAGGCTGGGTGAAGACCCTTA	TGAATGGCCGTTTCTGGAAGT	157
Gfap	GGGGCAAAAGCACCAAAGAAG	GGGACAACTTGTATTGTGAGCC	76
Tbp	AGAACAATCCAGACTAGCAGCA	GGGAACTTCACATCACAGCTC	120

158x256mm (300 x 300 DPI)

Suppl. Tab. 4 Statistical confidence intervals of flow cytometric data

Figure	Exp. group x-axis	CI type	CI values
Fig. 3B	Astrocytes	95% confidence interval	-3842 to 309,3
Fig. 3B	CD4+ T cells	96.83% CI of difference	7722 to 171354
Fig. 3B	Ma/acMi	96.83% CI of difference	368,9 to 304246
Fig. 3B	Other leukocytes II	96.83% CI of difference	20234 to 141660
Fig. 3B	Surface -	95% confidence interval	345,1 to 25902
Fig. 3B	Resting Microglia	95% confidence interval	2938 to 61315
Fig. 3B	Alt. acMi/Mo	96.83% CI of difference	-7057 to 334102
Fig. 3B	Other leukocytes I	96.83% CI of difference	-160,1 to 28985
Fig. 3C	GM-CSF+	96.83% CI of difference	5156 to 36052
Fig. 3C	IFNg+	95% confidence interval	-1491 to 17087
Fig. 3C	IL-17A	96.83% CI of difference	1400 to 19892
Fig. 3C	TNFa+	95% confidence interval	-5115 to 17226
Fig. 3D	GM-CSF+	95% confidence interval	-8,744 to 19,26
Fig. 3D	IFNg+	95% confidence interval	-11,64 to 7,552
Fig. 3D	IL-17A	95% confidence interval	2,565 to 7,475
Fig. 3D	TNFa+	95% confidence interval	-11,47 to 6,768
Fig. 3E	GM-CSF+	95% confidence interval	-0,08823 to 3,660
Fig. 3E	IFNg+	95% confidence interval	-0,1686 to 2,397
Fig. 3E	IL-17A	95% confidence interval	0,1249 to 1,563
Fig. 3E	TNFa+	95% confidence interval	-12,04 to 3,964

160x151mm (300 x 300 DPI)